Missouri S&T

Missouri University of Science and Technology
Scholars' Mine

Mechanical and Aerospace Engineering Faculty Research & Creative Works

Mechanical and Aerospace Engineering

01 Apr 2012

A Nanoporous Silicon Nitride Membrane Using A Two-step Lift-off Pattern Transfer With Thermal Nanoimprint Lithography

Bhargav P. Nabar

Zeynep Çelik-Butler

Brian H. Dennis

Richard E. Billo
Missouri University of Science and Technology, richard.billo@mst.edu

Follow this and additional works at: https://scholarsmine.mst.edu/mec_aereng_facwork

Part of the Aerospace Engineering Commons, and the Mechanical Engineering Commons

Recommended Citation

B. P. Nabar et al., "A Nanoporous Silicon Nitride Membrane Using A Two-step Lift-off Pattern Transfer With Thermal Nanoimprint Lithography," *Journal of Micromechanics and Microengineering*, vol. 22, no. 4, article no. 45012, IOP Publishing, Apr 2012.
The definitive version is available at https://doi.org/10.1088/0960-1317/22/4/045012

This Article - Journal is brought to you for free and open access by Scholars' Mine. It has been accepted for inclusion in Mechanical and Aerospace Engineering Faculty Research & Creative Works by an authorized administrator of Scholars' Mine. This work is protected by U. S. Copyright Law. Unauthorized use including reproduction for redistribution requires the permission of the copyright holder. For more information, please contact scholarsmine@mst.edu.

Journal of Micromechanics and Microengineering

PAPER

A nanoporous silicon nitride membrane using a two-step lift-off pattern transfer with thermal nanoimprint lithography

To cite this article: Bhargav P Nabar *et al* 2012 *J. Micromech. Microeng.* **22** 045012

View the article online for updates and enhancements.

You may also like

- Deposition of a-C:H films on a nanotrench pattern by bipolar PBII&D
Yuki Hirata, Yuya Nakahara, Keisuke Nagato et al.

- Micro-print and nano-imprint methods combining laser-drilled screen printing and ultraviolet nanoimprint lithography: a review
Masaru Nakagawa

- Self-aligned metallization on organic semiconductor through 3D dual-layer thermal nanoimprint
Y Jung and X Cheng

This content was downloaded from IP address 131.151.26.204 on 18/07/2023 at 19:55

J. Micromech. Microeng. 22 (2012) 045012 (8pp) doi:10.1088/0960-1317/22/4/045012

A nanoporous silicon nitride membrane using a two-step lift-off pattern transfer with thermal nanoimprint lithography

Bhargav P Nabar[1], Zeynep Çelik-Butler[1], Brian H Dennis[2] and Richard E Billo[3]

[1] Department of Electrical Engineering and Nanotechnology Research and Teaching Facility, University of Texas at Arlington, Arlington, TX 76019, USA
[2] Department of Mechanical and Aerospace Engineering, University of Texas at Arlington, Arlington, TX 76019, USA
[3] Department of Industrial and Manufacturing Engineering, University of Texas at Arlington, Arlington, TX 76019, USA

E-mail: zbutler@uta.edu

Received 7 July 2011, in final form 20 November 2011
Published 15 March 2012
Online at stacks.iop.org/JMM/22/045012

Abstract
Nanoimprint lithography is emerging as a viable contender for fabrication of large-scale arrays of 5–500 nm features. A fabrication process for the realization of thin nanoporous membranes using thermal nanoimprint lithography is presented. Suspended silicon nitride membranes were fabricated by low-pressure chemical vapor deposition (LPCVD) in conjunction with a potassium hydroxide-based bulk micromachining process. Nanoscale features were imprinted into a commercially available thermoplastic polymer resist using a prefabricated silicon mold. The pattern was reversed and transferred to a thin aluminum oxide layer by means of a novel two-stage lift-off technique. The patterned aluminum oxide was used as an etch mask in a CHF_3/He-based reactive ion etch process to transfer the pattern to silicon nitride. Highly directional etch profiles with near vertical sidewalls and excellent Si_3N_4/Al_2O_3 etch selectivity were observed. One micrometer thick porous membranes with varying dimensions of $250 \times 250\ \mu m^2$ to $450 \times 450\ \mu m^2$ and a pore diameter of 400 nm have been engineered and evaluated. Results indicate that the membranes have consistent nanopore dimensions and precisely defined porosity, which makes them ideal as gas exchange interfaces in blood oxygenation systems as well as other applications such as dialysis.

(Some figures may appear in colour only in the online journal)

1. Introduction

Nanoporous membranes fabricated from organic and inorganic materials have garnered widespread interest in the scientific community. Such membranes are primarily used for selective mass transfer [1–3]. Owing to their unique physical properties at nanometer scale dimensions, nanoporous membranes also find applications such as biosensing and chemical sensing [4–7].

Typical requirements for porous membranes are precise pore placement, uniform pore density over a wide area and mechanical robustness to withstand frequently encountered differential pressures and cyclic loadings. Pore blockage during either fabrication or operation and subsequent impedance to matter transfer is another common problem for porous membranes that must be addressed. Additional application-specific requirements such as pore depth, pore diameter, membrane surface energy and surface texture place stringent demands on the fabrication process. A number of techniques have been developed to meet these constraints with each offering unique advantages and drawbacks.

Fabrication of porous membranes using electron beam lithography [8] and focused ion beam [9] has been reported. Porous membranes with a pore diameter of 50 nm and

 © 2012 IOP Publishing Ltd Printed in the UK & the USA

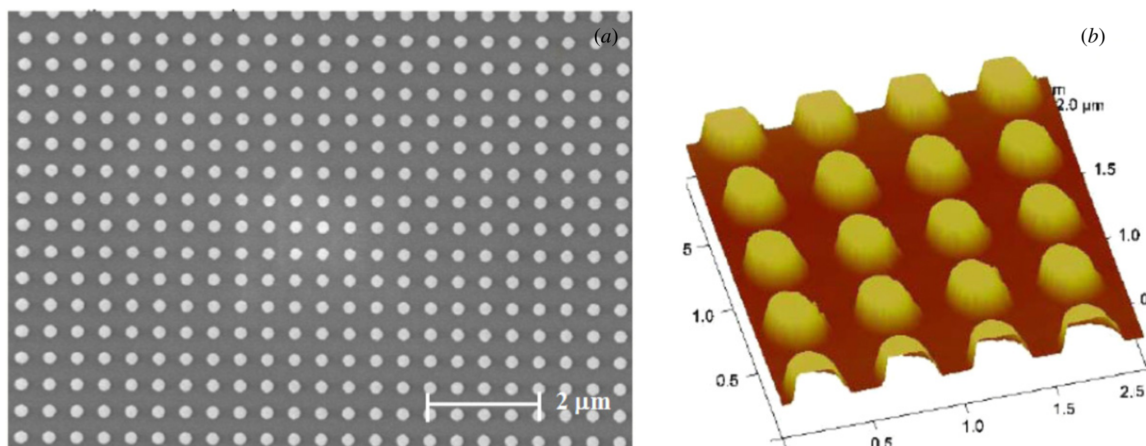

Figure 1. Silicon mold used for the nanoimprint lithography process. (*a*) SEM image. (*b*) AFM image. (Image courtesy of NILT, Denmark.)

1.8 μm have been achieved. These techniques offer significant advantages in terms of pore placement precision and the fabricated pores offer unimpeded mass transfer. Nevertheless, large-area production is not possible and as such, these techniques are impractical in terms of cost and time for mass fabrication of high-pore density membranes.

Heavy ion track etching is an established technique used to fabricate nanoporous membranes from organic polymers such as PCTE [10]. However, the inherent random nature of the heavy ions in the plasma environment precludes the formation of well-defined arrays of nanopores. Nanoporous membranes fabricated using interference lithography [11] have advantages such as uniform pore size and distribution, in addition to regular array arrangement of nanopores. The complexity of the process is the only limiting factor preventing widespread usage of the technique for porous membrane production.

Nanoimprint lithography (NIL), developed by Chou *et al* [12], provides an excellent solution to each of the shortcomings of the processes discussed above. NIL draws on the strengths of each of these processes and offers the advantage of being able to simultaneously fabricate a large number of nanoscale features with precise dimensions, high aspect ratio and accurate placement. Combined with conventional CMOS pattern transfer techniques, mass fabrication of wide-area arrays of nanometer features with high-aspect ratios is achievable at a fraction of the cost as compared to the other processes [13]. This makes NIL the method of choice for fabrication of nanoporous membranes in this present work.

The imprint resist used for NIL is typically a thermoplastic polymer such as PMMA. Such resists have been found to have limited etch resistance for dry etch processes [14]. These resists are better suited for lift-off-based techniques, which have been successfully demonstrated [5]. Another concern with NIL is the initial cost and complexity involved in the fabrication of the mold or the stamp. In order to adapt a fabricated silicon NIL mold designed for a direct etch process to a lift-off-based process, a two-stage lift-off process was developed. A similar technique has been previously demonstrated by Song *et al* [15] to obtain 146 nm diameter hole patterns of unspecified depth on a Si substrate. They have used UV-based nanoimprinting in their work. Here, we have utilized an alternate nanoimprinting method, namely thermal, and optimized the process to obtain through holes across a 1 μm thick Si_3N_4 membrane. This required precise pattern transfer accuracy across two lift-off processes and sufficient etch selectivity between the membrane and the etch mask to achieve holes with high-aspect ratios.

In this work, we present a fabrication technique for a bulk micromachined, nanoporous silicon nitride membrane containing a wide-area, highly periodic array of high-aspect ratio, through-membrane and straight-walled nanopores. We have used NIL in conjunction with a pattern reversal lithography technique, which is also described herein. Using the described process, we have been able to successfully fabricate 1 μm thick nanoporous silicon nitride membranes having a pore diameter of 400 nm with a pitch of 500 nm.

2. Experimental methods

2.1. Silicon mold

A three inch (1 0 0) silicon wafer patterned with pillar-shaped structures of 200 nm in diameter, 500 nm pitch and 120 nm in height was acquired from NILT technologies, Denmark (www.nilt.com). The dimensions of the mold features were chosen such that the resulting nanoporous membranes would have pore dimensions optimized for selective gas exchange between a liquid–gaseous interface. The mold was coated with a NXT 100 antiadhesion layer from Nanonex Inc. to facilitate separation of the mold from the nanoimprint resist after imprinting without damage (figure 1).

2.2. Silicon nitride growth and backside patterning

The process started with the deposition of a thin silicon nitride (Si_3N_4) layer. The Si_3N_4 was deposited using low-pressure chemical vapor deposition (LPCVD) on both sides of a 3″(1 0 0) silicon wafer at a temperature of 835 °C and a pressure of 250 mTorr. Dichlorosilane (100 sccm) and ammonia (20 sccm) were used as the process gases, resulting in growth of a 1 $\pm$ 0.05 μm thick low-stress Si_3N_4 at a rate of 200 nm h^{-1}. Next, NR9 3000P photoresist from Futurrex Inc. was spin coated on the backside to achieve a thickness

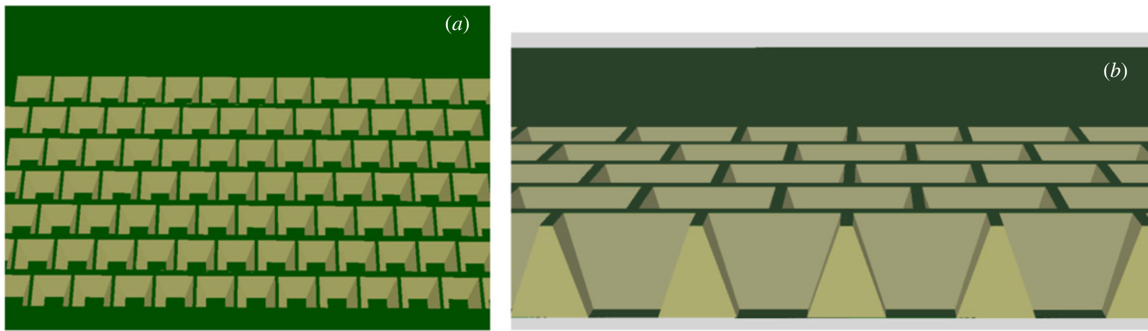

Figure 2. (*a*) Solid model showing the membrane array: green—Si_3N_4, brown—silicon. (*b*) Solid model cross section.

of 3 μm, followed by a prebake and UV exposure to define the membrane windows. After a postexposure, the resist was developed using the RD6 developer. As shown in figure 2, the pattern transferred from the photomask to the photoresist consisted of arrays of square-shaped features having dimensions of 250 × 250 μm^2, 350 × 350 μm^2 and 450 × 450 μm^2. These patterns were transferred from the photoresist to the underlying silicon nitride by means of a fluorine-based reactive ion etch (RIE) process, using tetrafluoromethane (CF_4) at 130 mTorr pressure, and 100 W RIE power. An etch rate of 30 nm min^{-1} was obtained.

2.3. Nanoimprint lithography and pattern reversal process

Nanoimprinting step started with spin coating a 180 nm thick NXR 1025 thermal imprint resist from Nanonex Inc. on the front-side silicon nitride. The wafer was then baked at 150 °C for 3 min on a hotplate to drive out all the solvent. The silicon nanoimprint mold was placed in contact with the nanoimprint resist and both wafers were loaded into a Nanonex NXB 200 nanoimprinter. The wafers were heated to a temperature of 130 °C and were compressed at an initial pressure of 120 psi. After holding the pressure constant for a few seconds, it was increased to 200 psi and thermal resist was imprinted for 30 s. Thereafter, the temperature was slowly reduced to room temperature, allowing the resist to solidify. The wafers were subsequently separated without much difficulty owing to the antiadhesion layer coated on the silicon mold. The resultant features are schematically illustrated in figure 3(*a*). The SEM photo is shown in figure 4(*a*).

The imprinting process resulted in an intentional residual resist with a thickness of 60–70 nm due to the difference in the thermal imprint resist thickness and the features on the mold. This residual resist was etched in a reactive ion etcher in Ar/O_2 plasma, at a pressure of 11 mTorr and with RF power of 40 W at 13.56 MHz to realize an anisotropic etch profile. Figures 3(*b*) and 4(*b*) depict the structures at the end of this stage.

Next, an 85 nm chromium layer was deposited on the thermal imprint resist in an electron beam evaporator, at a chamber pressure of 2.0 × 10^{-8} mTorr (figure 3(*c*)). The deposition rate was maintained at a constant 0.15 nm s^{-1} rate by means of controlling the electron beam current. This serves as an intermediary layer to transfer the pattern from the thermal resist to the aluminum oxide (Al_2O_3) mask layer. The Cr film was then patterned by means of a lift-off process in acetone bath, resulting in Cr pillars of 210 nm in diameter and 85 nm in height as shown in figures 3(*d*) and 4(*c*). After that, a thin film of Al_2O_3 was sputtered on top of the chromium pillars in an ultra-high vacuum RF magnetron sputter deposition system. The process pressure was set to 5.0 mTorr and the deposition was carried out at a RF power of 150.0 W. A total of 55 nm of Al_2O_3 was deposited at a deposition rate of 1.04 nm min^{-1} (figure 3(*e*)). Next, the Al_2O_3 was patterned by means of a second lift-off process, by placing the wafer in a CR 1020

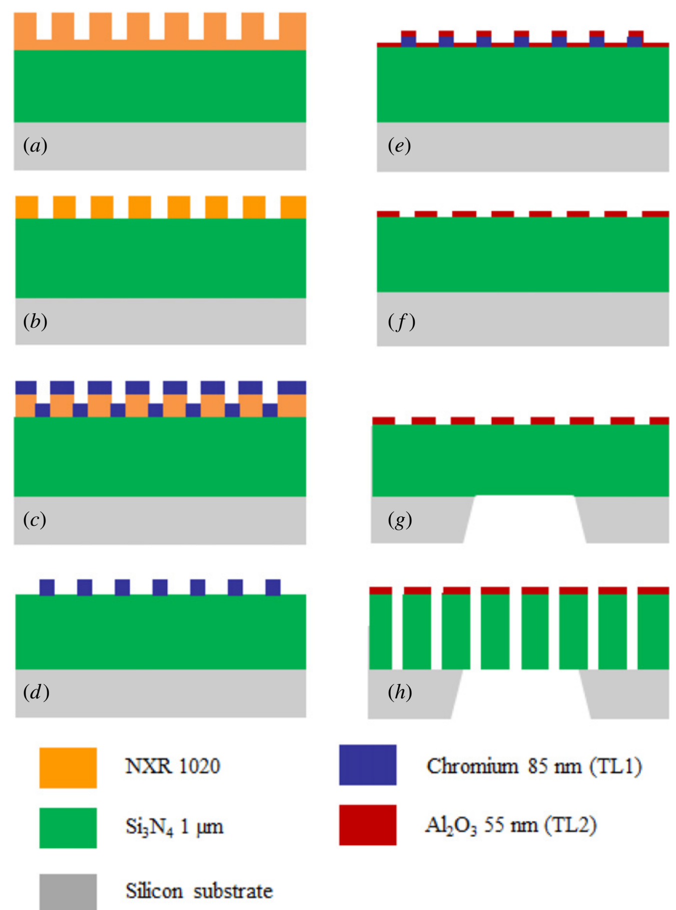

Figure 3. Schematic illustration of the nanoporous membrane fabrication process. (*a*) NXR1020 spin coating and nanoimprinting, (*b*) residual resist ashing, (*c*) chromium evaporation, (*d*) chromium lift-off, (*e*) aluminum oxide deposition, (*f*) aluminum oxide lift-off, (*g*) backside KOH etch, (*h*) reactive ion etch to realize nanopores.

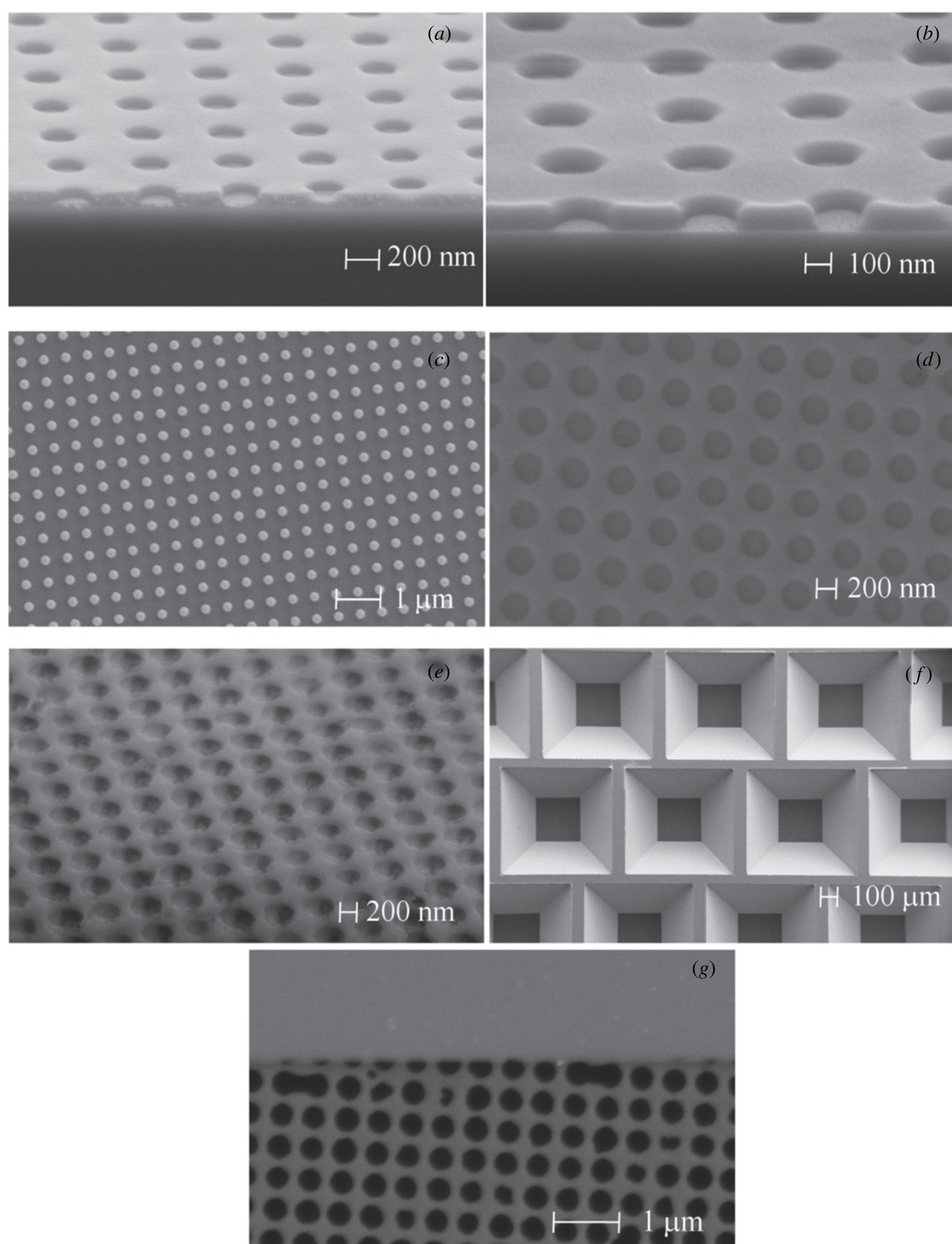

Figure 4. SEM images at different stages of the fabrication process. (*a*) NXR 1025 after nanoimprinting, (*b*) after residual resist ashing, (*c*) chromium lift-off, (*d*) aluminum oxide lift-off, (*e*) suspended nanoporous membrane from front side, zoomed-in view, (*f*) nanoporous membranes from backside, (*g*) zoomed-in image of suspended nanoporous membrane from the backside. The solid gray strip at the top denotes silicon.

Cr etchant bath. The process resulted in an array of circular patterns in the aluminum oxide layer having a diameter of 250 nm (figures 3(*f*) and 4(*d*)). The aluminum oxide layer was thus patterned over the entire area of the 3″ wafer except for 2 mm wide handling space along the wafer periphery.

2.4. Silicon nitride membrane and nanopore fabrication

The wafer was then subjected to a through-the-wafer potassium hydroxide (KOH) anisotropic wet etch process. The nanostructured aluminum oxide on the front side was protected from the KOH by clamping the wafer in a fixture specifically designed for the purpose. A steady etch rate of 1.2 μm min^{-1} was obtained at a temperature of 85.0 °C. The LPCVD Si_3N_4 was used as the etch stop. Suspended silicon nitride membranes having dimensions of 250 × 250 μm^2, 350 × 350 μm^2 and 450 × 450 μm^2 were thus obtained (figures 3(*g*) and 4(*f*)).

The patterned Al_2O_3 layer was used as the etch mask for the subsequent Si_3N_4 membrane etch. Using this mask, the 1 μm thick Si_3N_4 membrane was patterned in the fluorine-based RIE process with an inductively coupled plasma (ICP) generator at a process pressure of 11 mTorr. The ICP power was set to 4500 W and the wafer chuck was supplied with RF

power of 35 W. The process gases used were trifluoromethane (CHF_3) and helium (He). The etch process yielded a vertical etch rate of 63.8 nm min^{-1} for the LPCVD silicon nitride with sufficient anisotropy. Four hundred nanometer wide, 1 μm deep pores were obtained as a result of this etch process, as depicted in figure 3(*h*).

The complete fabrication process is schematically illustrated in figure 3. The SEM photos of nanoporous membrane reveal excellent periodicity and uniformity. From the SEM photos of the nanopores on the front-side (figure 3(*e*)) and the back-side (figure 3(*g*)), it is clear that the pores are all the way through the membrane.

3. Results and discussion

The two-stage lift-off pattern reversal technique described here was developed for two chief reasons. First, the nanoimprint resist did not possess sufficient selectivity over Al_2O_3 in a fluorine-based RIE process. Attempts to etch Al_2O_3 in a wet etch process with dilute hydrofluoric acid resulted in severe undercutting of the nanoimprint resist causing it to delaminate from the Al_2O_3 layer during the etch process. Therefore, it was concluded that a direct etch process would not be a feasible option for patterning of the Al_2O_3 layer. Indirect patterning using a conventional lift-off process would mean that the polarity of the silicon mold would have to be reversed, effectively necessitating fabrication of a new mold with holes instead of pillars. Such a mold, however, is harder to use due to difficulties in cleaning it, and would most likely to have a shorter life-time than a pillar mold because it would be more challenging to separate it from the resist after the nanoimprint process

Pattern reversal techniques for photolithography have been well established. These techniques were developed to provide an extra degree of flexibility to the process design engineer. By varying the photoresist processing parameters, the same photomask can be used for direct and reverse pattern transfer. The NIL pattern reversal technique accomplishes the same outcome by reversing the polarity of the pattern on the nanoimprint mold with the help of an intermediate etch mask deposited on the substrate. The pattern reversal is accomplished by means of two consecutive lift-off pattern transfer processes. This is illustrated in figure 3. The patterned nanoimprint resist is coated with a thin film of template layer 1(TL1). The first lift-off process is a conventional lift-off process that results in a mirror image of the mold pattern on the template layer 1. Next, the patterned template layer 1 is coated with a thin film of template layer 2 (TL2). The sample is then placed in an etchant to remove TL1. This results in patterning of TL2 by means of a lift-off. If this method were to be analogized to a conventional lift-off process, TL1 would be the 'lift-off resist' and the etchant would be the 'resist remover'.

The selection of TL2 is primarily governed by the requirements imposed by its function in the device or the fabrication process. In the present case, high etch selectivity over silicon nitride in a fluorine-based RIE process necessitated the selection of aluminum oxide as TL2. The

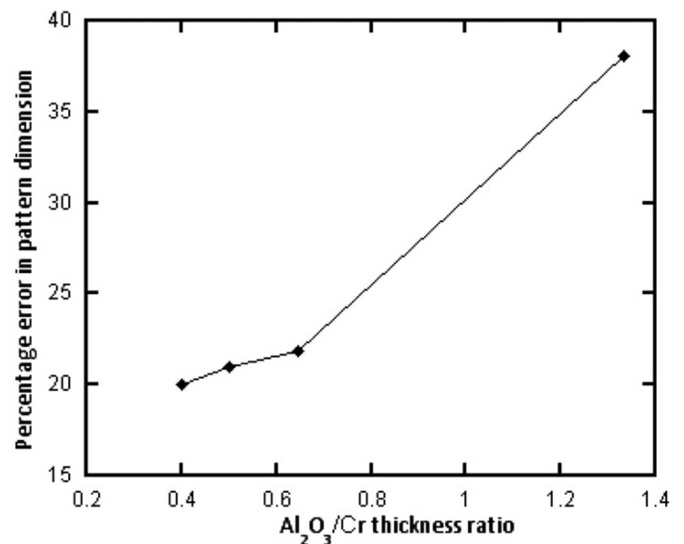

Figure 5. Percentage error in the nanopore dimension as a function of aluminum oxide to chromium thickness ratio.

two-stage lift-off process, however, imposes another important requirement on the selection of TL2, mainly that it should have sufficiently high-etch resistance to the chemical etchant used to remove TL1. A nontrivial etch rate for TL2 in the etchant can cause pattern distortion, as the removal process for TL1 is isotropic. Thus, TL1 has to be chosen such that it readily dissolves in a wet etchant that has a very low etch rate for TL2. In the present case, Al_2O_3 exhibited a negligible etch rate in CR 1020, the etchant used for removing chromium (etch rate 0.2 nm s^{-1}).

The thickness of TL1 could also be influenced by its role in the device/process. In addition, the ratio of thicknesses of TL2 to TL1 has been found to influence pattern transfer accuracy. As is observed in conventional lift-off processes, a high TL2 to TL1 thickness ratio leads to a larger error in the pattern dimension (figure 5).

This error could possibly stem from a conformal deposition of sputtered aluminum oxide on chromium. For a successful lift-off, any deposition of aluminum oxide on the sidewalls of the chromium pillar would first need to be removed for the etchant to access and dissolve chromium. Therefore, the time required for lift-off would be greater, considering that Al_2O_3 has a very slow etch rate in CR1020. It was observed that for Al_2O_3 to Cr thickness ratios greater than 0.4, the time required to dissolve Cr coated with Al_2O_3 was considerably more compared to that necessary to dissolve bare Cr of the same thickness. Moreover, ultrasonic agitation was necessary to achieve lift-off uniformity over the entire wafer. The greater time spent by the wafer in the etchant could cause pattern distortion of Al_2O_3. In general, the ideal method for deposition of TL2 would be one that is nonconformal, such as thermal or electron beam evaporation. In addition, if a lower thickness ratio of TL2 to TL1 can be tolerated, the resulting thinner sidewall would be easier to remove thus minimizing the error.

The sidewall profile of the Cr pillars was observed in a SEM by tilting the sample to 70°. The chromium pillars display a 'mushroom' like structure as seen in figure 6(*a*). The top half of the pillar is noticeably broader than the bottom.

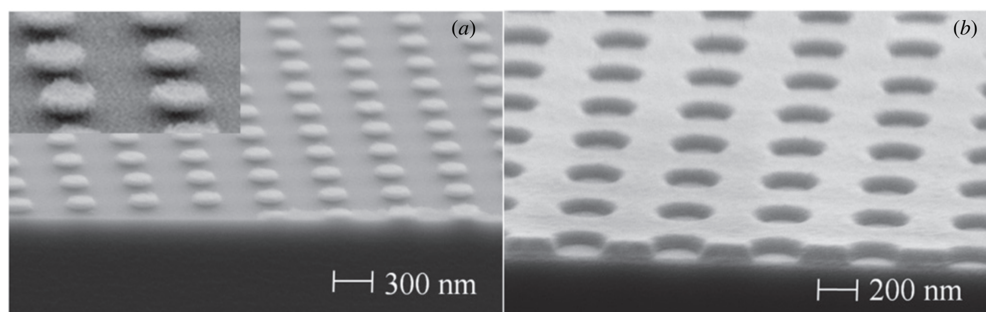

Figure 6. (*a*) Chromium lift-off stage showing 'mushroom' shaped pillars. Inset: magnified image. (*b*) Nanoimprint resist after residual resist ashing showing the positive sidewall profile.

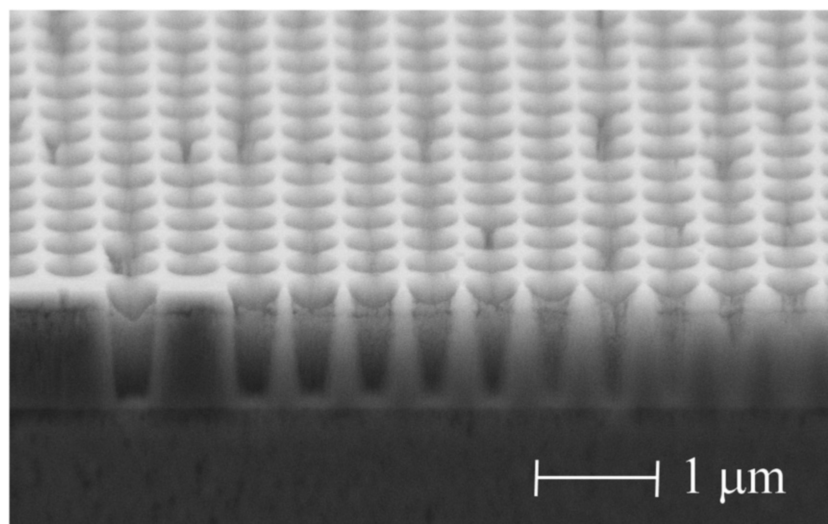

Figure 7. Reactive ion etch profile of nanopores in a 1 μm thick silicon nitride layer on silicon.

This is similar to a negative slope profile or an undercut profile typically observed in the sidewalls of conventional lift-off resists that are optimized for liftoff-based patterning. The mushroom structure causes a shadow effect during the deposition of Al_2O_3, thus minimizing the formation of an Al_2O_3 layer on the Cr pillar sidewall. The etchant can then access and remove the Cr in minimal time resulting in more accurate pattern transfer.

The negative sidewall slope in the chromium pillar is possibly an artifact of the Ar/O_2 etching process used for removing the residual resist after nanoimprinting. As seen in figure 6(*b*), the nanopore in the imprinted resist has a positive sidewall slope after residual resist etching. The positive sidewall slope in the imprint resist translates to a negative sidewall slope in the chromium pillar, resulting in the characteristic mushroom shape. It was observed that a ratio of 0.3 for the Al_2O_3/Cr thickness resulted in negligible distortion of the pattern dimensions. In addition, the time required for lift-off was significantly shorter and no ultrasonic agitation was necessary. The results point to the conclusion that pattern distortion in TL2 in the two-stage lift-off process can be limited by engineering of the sidewall profile of TL1 to obtain a negative sidewall slope.

Pattern transfer from the aluminum oxide to silicon nitride was achieved using a specially formulated RIE process. Trifluoromethane (CHF_3) was the primary etchant gas providing a source of fluorine radicals, while helium was added for dilution and to improve anisotropy. It was assumed that usage of a fluorine-deficient fluorocarbon such as trifluoromethane as opposed to tetrafluoromethane (CF_4) would limit the availability of fluorine radicals per unit volume of chamber atmosphere thus lowering the lateral etch rate and improving anisotropy [16]. Addition of helium-facilitated efficient transport of the reactant species and removal of volatile etch products. A low-chamber process pressure further improved the directionality, while independent control of the plasma density with the inductively coupled plasma generator improved selectivity. As shown in figure 7, near vertical sidewalls for the nanopores were obtained (sidewall angle 89.4°). The vertical to lateral etch rate ratio was 12.76 resulting in cylindrical pores with a pore diameter of 400 nm and a separation of 100 nm. The etch selectivity of Si_3N_4 to Al_2O_3 was found to be 24.75:1. To the best of our knowledge, the highest reported selectivity for silicon dioxide over silicon nitride is 30:1 in the plasma etch process [17]. Our results demonstrate the practicality of Al_2O_3 as an alternative mask for Si_3N_4 in a fluorine-based RIE process.

Postfabrication, the nanoporous membranes were examined for cracks and point defects. Figure 8(*a*) shows membrane placement and sampling locations on a 3″ diameter wafer.

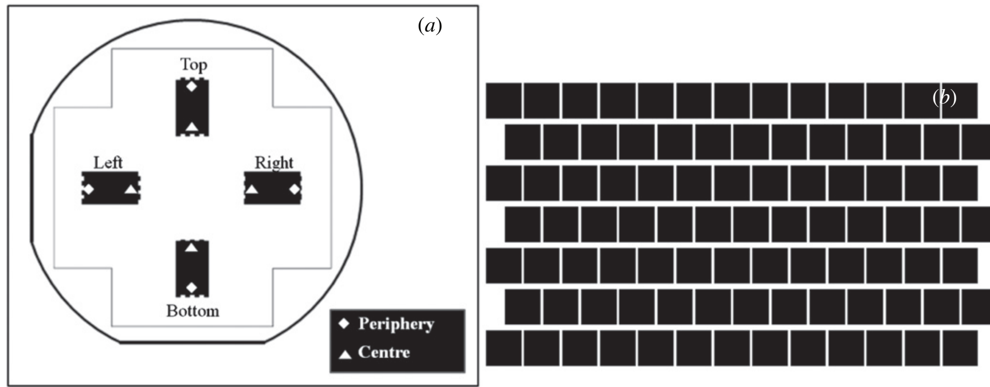

Figure 8. (*a*) Wafer layout and sampling location nomenclature. (*b*) Individual die.

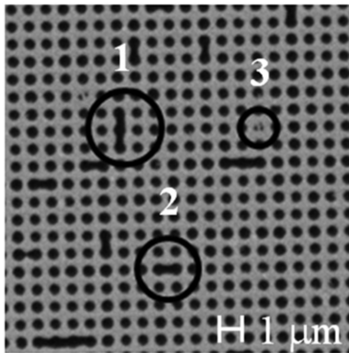

1. Defect event
2. Connected hole defect
3. Malformed hole defect.

Figure 9. Point defects on a 10 μm $\times$ 10 μm sample area of a suspended silicon nitride membrane.

Figure 8(*b*) shows an individual die on the wafer. Each die contains 91 suspended nanoporous membranes for a total of 364 membranes on the entire wafer. Each of the membranes was examined under a Nomarski microscope. All 364 membranes were found to be intact after the completion of the process.

A single membrane from each die—identified according to the nomenclature presented in figure 8(*a*)—was imaged using a scanning electron microscope for point defects. An area of 10 μm $\times$ 10 μm was chosen for characterization. Figure 9 shows the different point defects identified.

Observations at different points on the wafer as outlined by the nomenclature in figures 8(*a*) and 9 yielded the results shown in table 1.

The areal defect density was calculated as

$$\frac{\text{Area of a single pore} \times \text{average number of defective pores}}{\text{Sample area}}. \quad (1)$$

Accordingly, the areal defect density for the sampled areas was found to be 0.064. The observed standard deviation was significant at 27% and suggests that the detected

Table 1. Defect occurrences in 10 μm $\times$ 10 μm sample areas on a single wafer.

	Position of the sample area			
	Top	Bottom	Left	Right
Total no of pores	400	400	400	400
Defect events	13	27	24	22
Connected pores (*a*)	28	70	63	56
Malformed pores (*b*)	2	0	1	1
Total no. of damaged pores (*a*+*b*)	30	70	64	57
% Damaged pores	7.5	17.5	16	14.25
Wafer average% damaged pores	13.81			
% Standard deviation in no of damaged pores across wafer	27.66			

point defects are the result of randomly occurring process variations not inherent to the process design. Some of the identified process variations are local nonuniformities in the nanoimprint resist thickness from particulate residue and variations in the thickness of the nanoimprint resist after residual resist etching. Other reasons include artifacts from the nanoimprinting process due to local failure of the antiadhesion layer after repeated use and variations in the thickness of the Cr/Al_2O_3 resulting in improper lift-off. A significant reduction in the occurrences of point defects is thought to be possible by improving process environment and equipment repeatability such as that found in a commercial foundry.

The membranes were further characterized for variations in pore diameter across the wafer. The diameter was measured from images taken with a scanning electron microscope. The sampling locations were as illustrated in figure 8(*a*). A summary of the observations is presented in table 2.

As is evident from the per cent standard deviation, the variation in nanopore diameter is quite insignificant. The observations listed in table 2 also include human and instrument error in scanning electron microscopy, stemming from image focusing and diameter judgment from the obtained image using software-based analysis tools. As such, excellent uniformity in the nanopore diameter is observed across a 3″ wafer. This observation suggests that within the limits of reasonable process latitude, variation in nanopore diameter is more tolerant of the process variations listed previously. This demonstrates the efficacy of the two-step lift-off pattern

Table 2. Variation in nanopore diameter across a 3″ diameter wafer.

	Position							
	Top		Bottom		Left		Right	
	Center	Edge	Center	Edge	Center	Edge	Center	Edge
Average diameter (nm)	387	382	389	383	384	389	387	384
Wafer average (nm)	385.63							
% S.D	0.71							

transfer process toward pattern size uniformity over a large area.

4. Conclusion

Nanoporous silicon nitride membranes have been fabricated using thermal nanoimprint lithography in conjunction with a Cr-lift-off technique. Development of a novel two-stage lift-off process to accomplish pattern transfer from nanoimprint resist to silicon nitride is reported. A highly directional fluorine-based reactive ion-etch process for defining nanoscale dimensions is described. Viability of amorphous aluminum oxide as a suitable etch mask is demonstrated for reactive ion etching of silicon nitride. Nanoporous membranes of 1 μm thickness with highly ordered nanopores of 400 nm diameter have been achieved. The nanoporous membranes described in this work were meant to serve as gas exchange interfaces in blood oxygenation systems.

Acknowledgment

This work was in part supported by UTA/UTD/TI/THRE Medical Technology Research Program.

References

[1] Desai T, Hansford D, Leoni L, Essenpreis M and Ferrari M 2000 Nanoporous anti-fouling silicon membranes for biosensor applications *Biosens. Bioelectron.* **15** 453–62

[2] Fissel W, Humes H, Fleischman A and Roy S 2007 Dialysis and nanotechnology: now, 10 years, or never ? *Blood. Purif.* **25** 12–7

[3] Yang S, Ryu I, Kim H, Kim J, Jang S and Russell T 2006 Nanoporous membranes with ultrahigh selectivity and flux for the filtration of viruses *Adv. Mater.* **18** 709–12

[4] Heins E, Siwy Z, Baker L and Martin C 2005 Detecting single porphyrin molecules in a conically shaped synthetic nanopore *Nano. Lett.* **5** 1824–9

[5] Li Q, Luo G, Feng J, Zhou Q, Zhang L and Zhu Y 2001 Amperometric detection of glucose with glucose oxidase absorbed on porous nanocrystalline TiO_2 thin film *Electroanalysis* **13** 413–6

[6] Singh S, Arya S, Pandey P, Malhotra B, Saha S, Sreenivas K and Gupta V 2007 Cholesterol biosensor based on RF sputtered zinc oxide nanoporous thin film *Appl. Phys. Lett.* **91** 063901

[7] Ilwhan O, Monty C, Shannon M and Masel R 2007 Microfabricated electrochemical sensor for chemical warfare agents: smaller is better *Solid-State Sensors, Actuators and Microsystem Conf.* p 971

[8] Deshmukh M, Ralph D C, Thomas M and Silcox J 1999 Nanofabrication using a stencil mask *Appl. Phys. Lett.* **75** 1631–3

[9] Ambravaneswaran V, Uthamaraj S, Celik-Butler Z, Eberhart R, Chuong C, Billo R and Savitt M 2008 Micromachined nanoporous membranes for blood oxygenation systems *8th IEEE Conf. on Nanotechnology (Arlington, TX, USA)* p 201

[10] Ferain E and Legras R 1997 Characterization of nanoporous particle track etched membrane *Nucl. Instrum Methods Phys. Res.* B **131** 97–102

[11] Van Rijn C J M, Veldhuis G J and Kuiper S 1998 Nanosieves with microsystem technology for microfiltration applications *Nanotechnology* **9** 343–5

[12] Chou S, Krauss P and Renstrom P 1996 Nanoimprint lithography *J. Vac. Sci. Technol. B* **14** 4129–33

[13] Guo L J 2007 Nanoimprint lithography: methods and material requirements *Adv. Mater.* **19** 495–513

[14] Schulz H, Scheer H C, Hoomann T, Torres C M S, Pfeiffer K, Bleidiessel G, Cardinaud Ch, Peignon M C, Ahopelto J and Heidari B 2000 New polymer materials for nanoimprinting *J. Vac. Sci. Technol. B* **18** 1861

[15] Song S, Kim E, Jung H, Kim K and Jung G 2009 Reverse pattern duplication utilizing a two-step metal lift-off process via nanoimprint lithography *J. Micromech. Microeng.* **19** 105022

[16] Mele T C, Nulman J and Krusius J P 1984 Selective and anisotropic reactive ion etch of LPCVD silicon nitride with CHF_3 based gases *J. Vac. Sci. Technol. B* **2** 684–7

[17] Kastenmeier B E E, Matsuo P and Oehrlein G 1999 Highly selective etching of silicon nitride over silicon and silicon dioxide *J. Vac. Sci. Technol. A* **17** 3179–84